

# Molecular Dynamics Simulations of Polyelectrolyte–Polyampholyte Complexes. Effect of Solvent Quality and Salt Concentration

Junhwan Jeon<sup>†</sup> and Andrey V. Dobrynin<sup>\*,‡,§</sup>

Department of Chemical Engineering, Vanderbilt University, Nashville, Tennessee 37235, and Department of Physics and Polymer Program, Institute of Materials Science, University of Connecticut, Storrs, Connecticut 06269-3136

Received: July 7, 2006; In Final Form: September 25, 2006

Complexation between polyelectrolyte and polyampholyte chains in poor solvent conditions for the polyelectrolyte backbone has been studied by molecular dynamics simulations. In a poor solvent a polyelectrolyte forms a necklace-like structure consisting of polymeric globules (beads) connected by strings of monomers. The simulation results can be explained by assuming the existence of two different mechanisms leading to the necklace formation. In the case of weak electrostatic interactions, the necklace formation is driven by optimization of short-range monomer–monomer attraction and electrostatic repulsion between charged monomers on the polymer backbone. In the case of strong electrostatic interactions, the necklace structure appears as a result of counterion condensation. While the short-range attractions between monomers are still important, the correlation-induced attraction between condensed counterions and charged monomers and electrostatic repulsion between uncompensated charges provide significant contribution to optimization of the necklace structure. Upon forming a complex with both random and diblock polyampholytes, a polyelectrolyte chain changes its necklace conformation by forming one huge bead. The collapse of the polyelectrolyte chain occurs due to the neutralization of the polyelectrolyte charge by polyampholytes. In the case of the random polyampholyte, the more positively charged sections of the chain mix with negatively charged polyelectrolyte forming the globular bead while more negatively charged chain sections form loops surrounding the collapsed core of the aggregate. In the case of diblock polyampholyte, the positively charged block, a part of the negatively charged block, and a polyelectrolyte chain form a core of the aggregate with a substantial section of the negatively charged block sticking out from the collapsed core of the aggregate. In both cases the core of the aggregate has a layered structure that is characterized by the variations in the excess of concentration of monomers belonging to polyampholyte and polyelectrolyte chains throughout the core radius. These structures appear as a result of optimization of the net electrostatic energy of the complex and short-range attractive interactions between monomers of the polyelectrolyte chain.

## 1. Introduction

Electrostatic interactions control molecular process in different areas of natural sciences ranging from biophysics to materials science.<sup>1–5</sup> For example, electrostatic attractions between negatively charged DNA and net positively charged histones are responsible for the packaging of DNA into chromosomes.<sup>2,6–8</sup> The complexation of DNA with positively charged polyelectrolytes, dendrimers, colloidal particles, and liposomes facilitates the uptake of the DNA through the cell membrane and is utilized for gene therapy.<sup>4</sup> Electrostatic interactions between multivalent ions and DNA molecules, actin filaments, and tobacco mosaic viruses are the driving forces behind their assembly into compact bundle structures.<sup>7,9–21</sup>

Electrostatic attraction between oppositely charged macromolecules is a foundation of the electrostatic assembly technique that allows fabrication of multilayer films from synthetic polyelectrolytes, proteins, DNA, nanoparticles, etc.<sup>5,22,23</sup> A typical experimental procedure involves exposure of a solid

substrate to dilute solutions of positively or negatively charged species for a period of time optimized for their adsorption followed by a rinsing step to remove all loosely adsorbed material. Further film growth is achieved by alternating deposition of polyanions and polycations from their solutions. Inside the film oppositely charged molecules form complex-like multichain aggregates.<sup>5</sup>

The electrostatic driven complexation between oppositely charged macromolecules in solutions is utilized for protein separation.<sup>3,4,8,24</sup> In this case, flexible synthetic polyelectrolytes are added to aqueous protein solutions. Polyelectrolytes form complexes with proteins, which then precipitate from the solution. The binding between polyelectrolytes and proteins occurs in such a way that oppositely charged amino acids on the protein are close to the polyelectrolyte backbone, causing an electrostatic attraction between the two and resulting in the so-called polarization induced attraction mechanism for complex formation.<sup>25</sup> The electrostatic nature of association between polyelectrolytes and proteins is supported by the strong effect of pH and salt concentration on the complex stoichiometry and structure.<sup>3,4,8</sup> Another factor that can influence the affinity between proteins and polyelectrolytes is the counterion release

\* Address correspondence to this author. E-mail: avd@ims.uconn.edu.

<sup>†</sup> Vanderbilt University.

<sup>‡</sup> Department of Physics, University of Connecticut.

<sup>§</sup> Polymer Program, University of Connecticut.

from the polyelectrolytes. For example, if net positively charged proteins with an excess of the positively charged amino acid groups over negatively charged ones bind to anionic polyelectrolytes, the positively charged groups of the protein partially neutralize the polyelectrolyte charge allowing the release of counterions that reduce the charge of the polyelectrolytes in the absence of the proteins.<sup>3,4</sup> Substitution of the counterions by positively charged groups of the protein provides an additional entropic contribution to complex binding free energy.

Over the years molecular simulations of polyelectrolyte–protein (polyampholyte) mixtures were very helpful in elucidating factors controlling complex formation.<sup>25–31</sup> However, previous molecular simulations have ignored the effect of the solvent quality for the polyelectrolyte backbone on the complexation between polyampholyte and polyelectrolyte chains. Solvent quality for the polymer backbone plays an important role in determining the structure of a polyelectrolyte chain in solution. Polyelectrolytes in a poor solvent form a necklace-like structure of beads connected by strings of monomers.<sup>32–41</sup> This structure optimizes contributions of the short-range monomer–monomer and electrostatic interactions. As polymer concentration increases, the fraction of the condensed counterions on the chain increases and the chain shrinks by decreasing the length of the strings and number of beads per chain.<sup>39–41</sup> Thus, condensed counterions reduce effective charge on the polyelectrolyte chain altering its conformation. A similar effect on chain conformation can be achieved either by changing the salt concentration or by adding polyampholyte chains to the solution. In the former case, the increase of the salt concentration lowers the entropic penalty for counterion localization near the polyelectrolyte backbone. In the later case, complexation of the polyampholyte chain with a polyelectrolyte leads to neutralization of the polyelectrolyte charge. In both cases, the reduction of polyelectrolyte charge triggers conformational transformations in the polyelectrolyte chain. In this paper we use molecular dynamics simulations to study the effect of the salt concentration and the strength of the electrostatic interactions on conformations of a polyelectrolyte chain in poor solvent conditions for the polymer backbone and its complexation with symmetric polyampholytes of net zero charge.

## 2. Model and Simulation Details

We performed molecular dynamics simulations of complexation between hydrophobic polyelectrolyte (PE) and polyampholyte (PA) chains. Both chains are modeled as bead-spring chains of charged Lennard-Jones particles with diameter  $\sigma$  and consisting of  $N_{\text{PE}} = 187$  and  $N_{\text{PA}} = 186$  beads. Every third bead on the polyelectrolyte chain is carrying a negative elementary charge,  $-e$ . This corresponds to the fraction of charged monomers,  $f$ , on the polymer backbone equal to  $f = 1/3$ . All beads of polyampholyte are positively or negatively charged with the net polymeric charge being equal to zero. We studied polyampholytes with random (RPA) and diblock charge sequences along the polymer backbone.

The connectivity of beads into polymer chains is maintained by the finite extension nonlinear elastic (FENE) potential

$$U_{\text{FENE}}(r) = -0.5k_{\text{spring}}R_{\text{max}}^2 \ln\left(1 - \frac{r^2}{R_{\text{max}}^2}\right) \quad (1)$$

where  $k_{\text{spring}}$  is the spring constant set to be  $k_{\text{spring}} = 7k_{\text{B}}T/\sigma^2$  and the maximum bond length is  $R_{\text{max}} = 2\sigma$ ,  $k_{\text{B}}$  is the Boltzmann constant, and  $T$  is the absolute temperature.

**TABLE 1: Interaction Parameters Used in Simulations**

pairs	$\epsilon_{\text{LJ}} (k_{\text{B}}T)$	$r_{\text{cut}} (\sigma)$
PE monomer–PE monomer	1.5	2.5
PA monomer–PA monomer	0.35	2.5
PE monomer–PA monomer	$\sqrt{(1.5 \times 0.35)}$	2.5
PE monomer–counterion	1.0	$\sqrt[9]{2}$
PA monomer–counterion	1.0	$\sqrt[9]{2}$
counterion–counterion	1.0	$\sqrt[9]{2}$

Electrostatic interaction between any two charged particles bearing the charge valences  $q_i$  and  $q_j$ , and separated by a distance  $r_{ij}$ , is given by the Coulomb potential

$$U_{\text{Coul}}(r_{ij}) = k_{\text{B}}T \frac{l_{\text{B}}q_iq_j}{r_{ij}} \quad (2)$$

The strength of the electrostatic interactions is determined by the value of the Bjerrum length  $l_{\text{B}} = e^2/\epsilon k_{\text{B}}T$ , which is defined as the length scale at which the Coulomb interaction between two elementary charges  $e$  in a dielectric medium with the dielectric constant  $\epsilon$  equal to the thermal energy  $k_{\text{B}}T$ . For example, the Bjerrum length is about 7 Å in water at room temperature, 298 K. In our simulations, the value of the Bjerrum length  $l_{\text{B}}$  is equal to  $1\sigma$ ,  $2\sigma$ , and  $3\sigma$ . The system electroneutrality is maintained by adding monomer-like counterions to compensate for each charge on the polyampholyte and polyelectrolyte chains. In addition to counterions we have also added salt ions with concentration varying between 0 and  $(1.25 \times 10^{-3})\sigma^{-3}$ . Zero salt concentration means that there are only counterions in the systems. All charged particles in our simulations are monovalent ions with valence  $q_i = \pm 1$ .

In addition to electrostatic interactions both charged and uncharged particles in the system interact through the truncated-shifted Lennard-Jones potential

$$U_{\text{LJ}}(r_{ij}) = \begin{cases} 4\epsilon_{\text{LJ}} \left[ \left( \frac{\sigma}{r_{ij}} \right)^{12} - \left( \frac{\sigma}{r_{ij}} \right)^6 - \left( \frac{\sigma}{r_{\text{cut}}} \right)^{12} + \left( \frac{\sigma}{r_{\text{cut}}} \right)^6 \right] & r \leq r_{\text{cut}} \\ 0 & r > r_{\text{cut}} \end{cases} \quad (3)$$

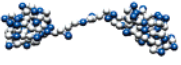
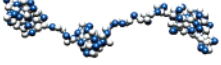
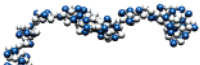
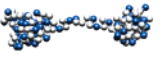
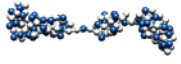
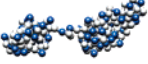
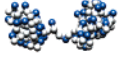
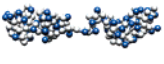
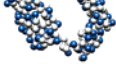
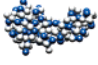
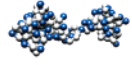
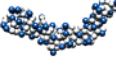
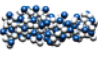
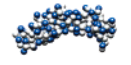
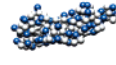
where  $r_{ij}$  is the distance between two interacting  $i$ th and  $j$ th beads,  $\sigma$  is the bead diameter, which is chosen to be the same regardless of the type of beads, and  $r_{\text{cut}}$  is a cutoff distance beyond which the interactions are ignored. The interaction parameters for LJ interactions are summarized in Table 1. The choice of the LJ parameters for the polyelectrolyte and polyampholyte chains corresponds to poor and  $\theta$  solvent conditions for the polyelectrolyte and polyampholyte backbones, respectively.

Simulations are carried out in a constant number of particles, constant volume, and constant temperature (NVT) ensemble with periodic boundary conditions and simulation box size  $L = 123.2\sigma$ . This corresponds to a polyelectrolyte concentration  $c = 10^{-4}\sigma^{-3}$ . The electrostatic interactions in our simulations are calculated by the Particle-Particle Particle-Mesh (P<sup>3</sup>M) method<sup>42–44</sup> implemented in LAMMPS,<sup>45</sup> which takes into account electrostatic interactions with all periodic images of the system.

The constant temperature is maintained by coupling the system to the Langevin thermostat.<sup>45</sup> In this case, the motion of beads in the system is described by the following equation

$$m \frac{d\vec{v}_i(t)}{dt} = \vec{F}_i(t) - \xi \vec{v}_i(t) + \vec{F}_i^R(t) \quad (4)$$

**TABLE 2: Typical Conformations of Polyelectrolyte Chains<sup>a</sup>**

Salt concentration ( $c_s$ )	$l_B = 1\sigma$	$l_B = 2\sigma$	$l_B = 3\sigma$
0			
$5 \times 10^{-5}$			
$2.5 \times 10^{-4}$			
$5 \times 10^{-4}$			
$1.25 \times 10^{-3}$			

<sup>a</sup> The negatively charged monomers of a polyelectrolyte chain are blue and neutral monomers are gray.

where  $m$  is the bead mass,  $\vec{v}_i$  is the bead velocity, and  $\vec{F}_i$  denotes the net deterministic force acting on the  $i$ th bead. The stochastic force  $\vec{F}_i^R$  has a zero average value  $\langle \vec{F}_i^R(t) \rangle = 0$  and  $\delta$ -functional correlations  $\langle \vec{F}_i^R(t) \vec{F}_i^R(t') \rangle = 6k_B T \xi \delta(t - t')$ . The friction coefficient  $\xi$  was set to  $\xi = m/\tau_{LJ}$ , where  $\tau_{LJ}$  is the standard LJ time  $\tau_{LJ} = \sigma(m/\epsilon_{LJ})^{1/2}$ . The velocity-Verlet algorithm<sup>42</sup> with a time step  $\Delta t = 0.01 \tau_{LJ}$  was used for integration of the equations of motion (4).

Simulations were performed by using the following procedure: In the case of polyelectrolyte chain simulations at the beginning of each simulation run, a negatively charged polyelectrolyte chain in self-avoiding walk configuration was placed in the center of the simulation box together with its counterions and salt ions. The system was preequilibrated for  $1 \times 10^6$  MD steps. This was followed by the production run lasting  $3 \times 10^6$  MD steps. During the production run we averaged the distribution functions of the number of monomers in beads and strings, the distribution function of the number of beads per chain, the chain radius of gyration, the form factor of a polyelectrolyte chain, and the small ion's density distribution functions. For simulations of the complex formation between polyelectrolyte and polyampholyte chains, at the beginning of each simulation run, a preequilibrated polyampholyte chain was placed at a distance of the order of its radius of gyration from the polyelectrolyte backbone. The simulation run was continued for  $4 \times 10^6$  MD steps and the final  $3 \times 10^6$  MD steps were used for the data collection.

### 3. Effect of Added Salt on Conformations of a Polyelectrolyte Chain

In this section we discuss how salt concentration and strength of the electrostatic interactions influence polyelectrolyte chain conformations. In a poor solvent condition for the polymer backbone, a polyelectrolyte chain adopts a necklace-like conformation of beads connected by strings of monomers (see Table 2). The necklace parameters such as the number of beads, number of monomers in a bead, bead size, number of monomers in a string, and string length depend on the strength of the electrostatic interactions and salt concentration. The distribution functions presented below were obtained by utilizing the

necklace structure analysis algorithm described in the Appendix of ref 41. Panels a and b of Figure 1 show distribution functions of the number of beads per chain for two systems with the value of the Bjerrum length  $l_B = 3\sigma$  and  $1\sigma$ . Note that the counterion concentration in these simulations was kept constant and equal to  $c_c = (3.37 \times 10^{-5})\sigma^{-3}$ . The three-bead necklace is the most probable chain conformation for the system with the value of the Bjerrum length  $l_B = 3\sigma$  at zero salt concentration (see also Table 2). As salt concentration increases the probability of the necklaces with  $n_b > 2$  decreases while necklaces with two beads become more favorable. A sausage-like aggregate appears in the systems with high probability at  $c_s \approx (5 \times 10^{-4})\sigma^{-3}$  for both systems (see Table 2) and continues to dominate the chain conformations as salt concentration increases further.

Panels a and b of Figure 2 show the dependence of the number of monomers per bead for the systems with the value of the Bjerrum  $l_B = 3\sigma$  and  $1\sigma$  at different salt concentrations. At zero salt concentration ( $2c_s + c_c = (3.37 \times 10^{-5})\sigma^{-3}$ ) for the system with  $l_B = 3\sigma$ , there are three beads on the necklace, which is indicated by the existence of the two peaks in the distribution functions of the number of monomers in a bead (see Figure 2 a). The broad peak centered at  $m_b \approx 50$  corresponds to two beads formed at the ends of the polymer chain. The additional small peak located at  $m_b \approx 10$  is due to a smaller bead formed in the middle of the chain. As salt concentration increases, the peak corresponding to a middle bead disappears and the necklace preferentially has two beads that are formed on the chain ends. With increasing salt concentration, this peak shifts toward larger  $m_b$  values and broadens, while its amplitude decreases. The distribution function of the number of monomers in a bead for the system with the Bjerrum length  $l_B = 1\sigma$  shown in Figure 2b has a peak at  $m_b \approx 76$ . As salt concentration increases, these two beads grow in size by absorbing monomers belonging to the string. There are about 35 monomers left to form a string connecting these two beads. By absorbing these monomers into beads, each bead can only increase the number of monomers in a bead by no more than 17 monomers. Thus, the weak salt concentration dependence of the peak position in the number of monomers in a bead



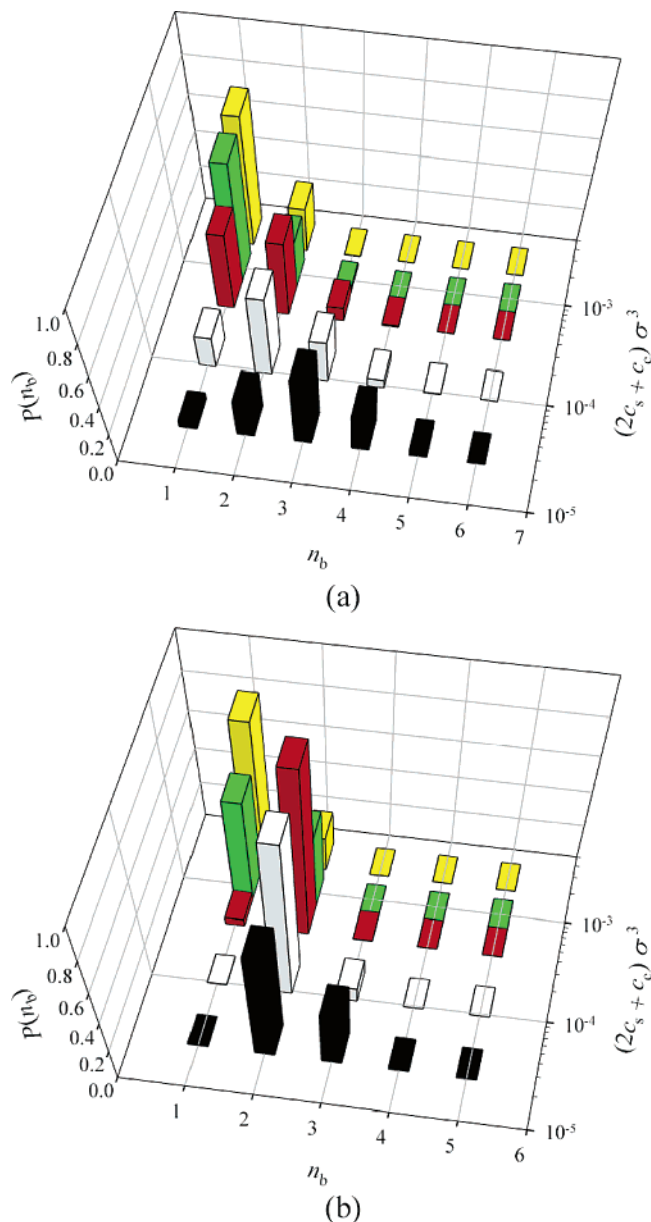


**Figure 1.** Distribution function of the number of beads per chain for polyelectrolyte with  $f = 1/3$  and  $N_{PE} = 187$  at different salt concentrations and different values of the Bjerrum length (a)  $l_B = 3\sigma$  and (b)  $l_B = 1\sigma$ .

distribution function as seen in Figure 2b is a result of the finite number of monomers in a polyelectrolyte chain.

A polyelectrolyte chain can also adopt a sausage-like conformation (see Table 2). This conformation corresponds to a peak in the distribution function located at  $m_b = 187$ . The appearance of this peak is a result of exchange of monomers between beads and strings. With increasing salt concentration, electrostatic repulsion between beads on the chain decreases resulting in a smaller number of monomers in strings,  $m_s$  (see Figures 3), and subsequently a low energetic barrier for the exchange of monomers between beads and strings. Thus, the variations in the bead distribution function are associated with the counterion condensation and screening of the electrostatic interactions by salt ions. The entropic penalty for the counterion localization inside beads decreases with increasing salt concentration  $c_s$  resulting in the larger number of counterions residing inside beads reducing their effective charge. It is interesting to point out that the maximum in the string distribution function

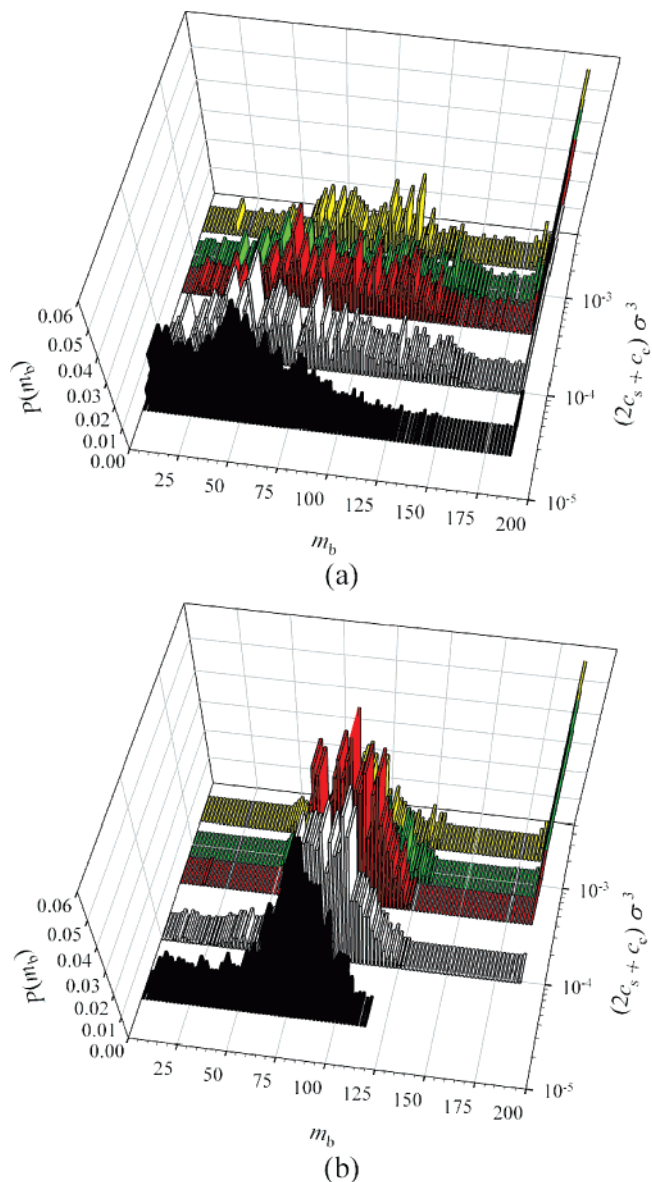


**Figure 2.** Distribution function of the number of monomers in a bead at different salt concentrations and different values of the Bjerrum length (a)  $l_B = 3\sigma$  and (b)  $l_B = 1\sigma$ .

for the salt-free system with the Bjerrum length  $l_B = 1\sigma$  is shifted toward the optimal string size of the three-bead necklace (see Figure 3b). This is due to coexistence of the three-bead necklaces with two-bead necklaces at this salt concentration (see Figure 1b). For any three-bead necklace there are two strings connecting three beads and the frequency of finding such strings is twice the frequency of finding a necklace with three beads. However, the probability of finding longer strings connecting larger beads in two-bead necklaces is proportional to the probability of finding a two-bead necklace. This could lead in some special cases to a shift of the maximum in the string distribution function toward shorter strings as is seen in Figure 3b.

There are two different mechanisms that can lead to formation of the necklace structure.<sup>41</sup> The first one is competition between solvophobic (hydrophobic) and electrostatic interactions. The second mechanism is mainly electrostatic in nature and is due to competition between correlation-induced attraction existing in condensed counterions and electrostatic repulsion between uncompensated charges on the polymer backbone. By changing the strength of the electrostatic interactions (changing the value

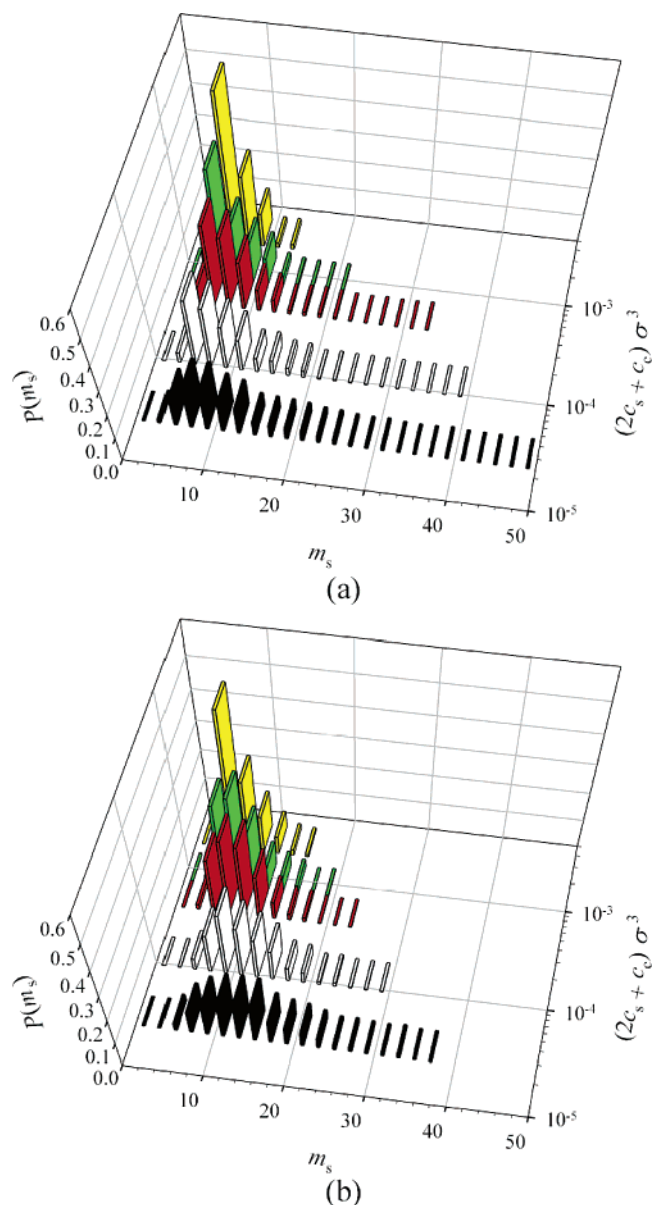


**Figure 3.** Distribution function of the number of monomers in a string at different salt concentrations and different values of the Bjerrum length (a)  $l_B = 3\sigma$  and (b)  $l_B = 1\sigma$ .

of the Bjerrum length) one can obtain necklaces formed either by the first or by the second mechanism.

The optimal number of monomers in a bead  $m_b^*$  is determined by balancing the interfacial energy of a bead of size  $D_b$

$$F_{\text{surf}} \approx \gamma D_b^2 \quad (5)$$

where  $\gamma$  is the interfacial energy of the globular interface, with the bead's electrostatic energy  $F_{\text{elec}}$ . The electrostatic energy of a bead containing  $m_b^*$  monomers and having  $xm_b^*$  condensed counterions in it is estimated as

$$F_{\text{elec}} \approx k_B T \frac{l_B ((1-x)fm_b^*)^2}{D_b} \quad (6)$$

where  $f$  is the fraction of charged monomers on the polymer backbone and  $x$  is the fraction of condensed counterions inside a bead. Note that the problem of the stability of the charged bead is similar to the classical problem of the instability of a charged droplet, considered by Lord Rayleigh over one hundred

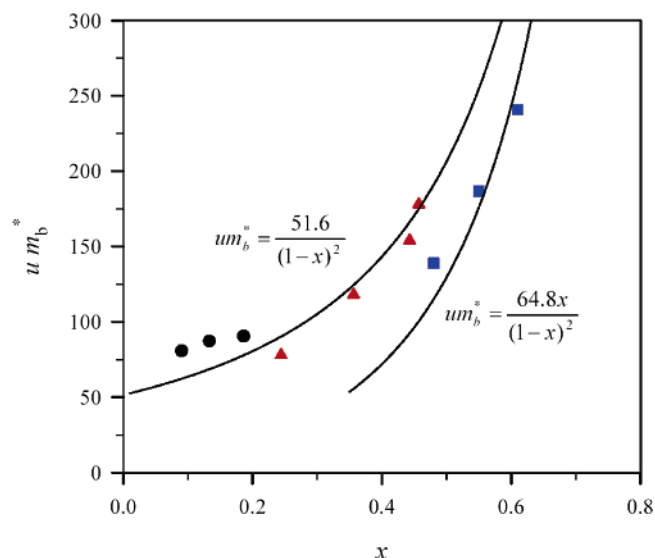


**Figure 4.** Dependence of the parameter  $um_b^*$  on the fraction of condensed counterions,  $x$ , at different salt concentrations for the systems with  $l_B = 1\sigma$  (filled circles),  $2\sigma$  (filled triangles), and  $3\sigma$  (filled squares). Solid lines are the best fits to eqs 7 and 8.

years ago. In his classical experiments Rayleigh had shown that a charged droplet is unstable and breaks into smaller droplets if its charge exceeds some critical value  $Q_{\text{crit}}$ . The equilibrium state of the charged droplet with  $Q > Q_{\text{crit}}$  is a set of smaller droplets with the charge on each of them smaller than the critical one and placed at infinite distance from each other.

The different mechanisms for the chain collapse lead to different expressions for the equilibrium monomer density inside bead  $\rho$ , a different equation for the bead interfacial energy  $\gamma$ , and a different relationship between number of monomers in a bead  $m_b^*$  and its size  $D_b$ . In the case when solvophobic (hydrophobic) interactions cause chain collapse, the equilibrium density inside a bead is determined by balancing the two-body attraction with three-body repulsion (see for details see ref 41). The equilibrium monomer density inside such a globule is equal to  $\rho \approx |\tau|/\sigma^3$ , where  $\tau = (1 - \theta/T)$  is the effective temperature characterizing the proximity of the system to the  $\theta$  temperature. The bead size is related to the number of monomers in it by the following equation:  $D_b \approx (m_b/\rho)^{1/3} \approx \sigma m_b^{1/3}/|\tau|^{1/3}$ . The interfacial energy  $\gamma$  of the globule is equal to  $k_B T |\tau|^2/\sigma^2$ . The optimal bead size for this system is given by the following equation

$$m_b^* \approx \frac{|\tau|}{uf^2(1-x)^2}, \text{ solvophobic interactions} \quad (7)$$

where  $u$  is the ratio of the Bjerrum length  $l_B$  to the bond length  $\sigma$ . It follows from eq 7 that the size of the bead increases with increasing the fraction of the condensed counterions  $x$ .

In the case of strong electrostatic interactions, the equilibrium density inside a bead is determined by balancing the correlation-induced attraction between condensed counterions and charged monomers and three-body monomer–monomer repulsion (see for details ref 41). The equilibrium density inside a globule is equal to  $\rho \approx u^{3/5}(xf)^{4/5}/\sigma^3$  and its interfacial energy is  $\gamma \approx k_B T u^{8/5}(xf)^{9/5}/\sigma^2$ . The optimal number of monomers in a bead is obtained by balancing electrostatic and surface energies of the bead

$$m_b^* \approx \frac{x}{f(1-x)^2}, \text{ correlation-induced attraction} \quad (8)$$

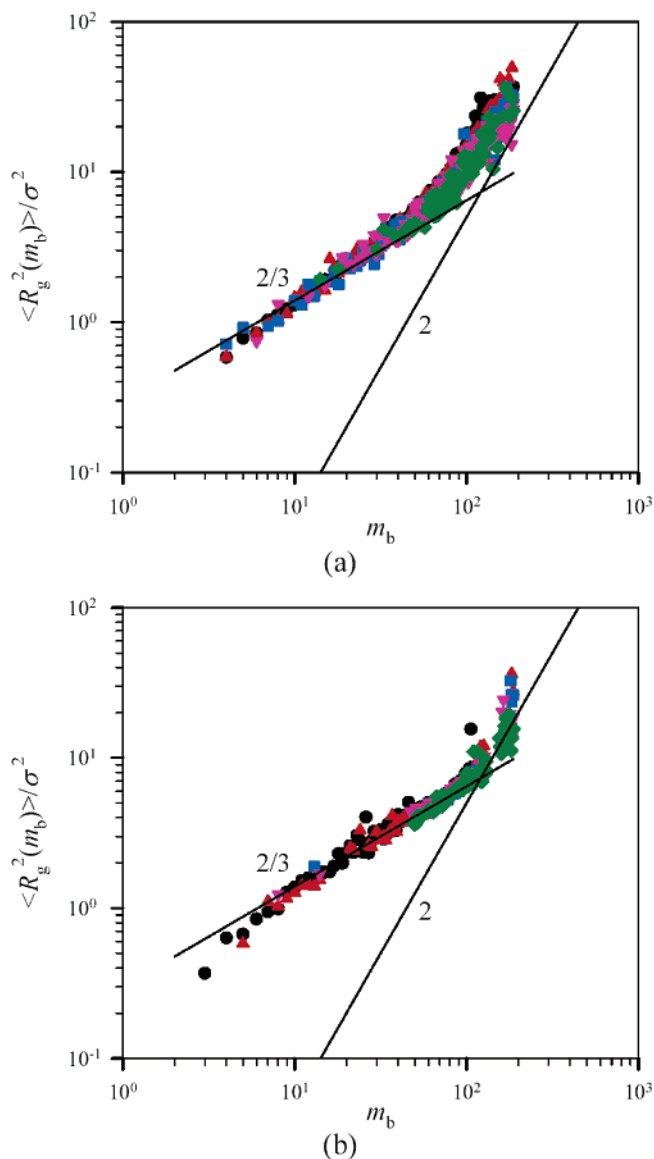


**Figure 5.** Dependence of the mean-square radius of gyration of an aggregate on the number of monomers in it for different values of the Bjerrum length (a)  $l_B = 3\sigma$  and (b)  $l_B = 1\sigma$  and at different salt concentrations:  $c_s = 0\sigma^{-3}$  (filled circles),  $(5 \times 10^{-5})\sigma^{-3}$  (filled triangles),  $(2.5 \times 10^{-4})\sigma^{-3}$  (filled squares),  $(5 \times 10^{-4})\sigma^{-3}$  (filled reverse triangles), and  $(1.25 \times 10^{-3})\sigma^{-3}$  (filled diamonds).

The transition between two different collapse mechanisms takes place when the densities inside beads are of the same order in magnitude,  $|\tau| \approx u^{3/5}(xf)^{4/5}$ . Thus, in the range of parameters,  $xf > |\tau|^{5/4}/u^{3/4}$ , the correlation-induced attraction is stronger than two-body attraction and controls the equilibrium bead size. Thus, by changing the value of the Bjerrum length  $l_B$  and salt concentration, one can explore different collapse regimes of the necklace-like globule.

Equations 7 and 8 give simple relations between the optimal number of monomers in a bead and the fraction of condensed counterions,  $x$ . Note that in our evaluation of the number of condensed counterions we have included both the polyelectrolyte counterions and positively charged salt ions that condensed on the beads. We tested these relations for polyelectrolyte chains with different strengths of the electrostatic interactions and different salt concentrations (see Figure 4). To improve statistics each point is averaged over all beads with the number of monomers,  $m_b$ , within five monomers of the most probable (optimal) number of monomers in a bead ( $m_b^* - 5 \leq m_b \leq$

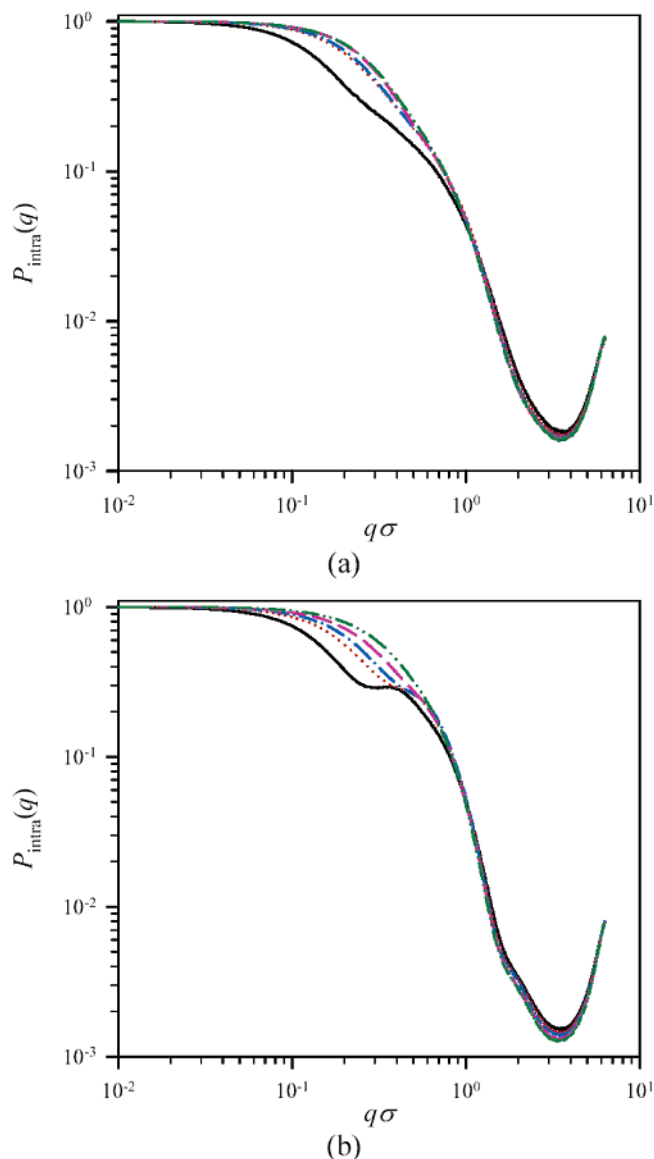


**Figure 6.** Form factor of a polyelectrolyte chain with degree of polymerization  $N_{PE} = 187$  and fraction of charged monomers  $f = 1/3$  for different values of the Bjerrum length (a)  $l_B = 3\sigma$  and (b)  $l_B = 1\sigma$  and different salt concentrations:  $c_s = 0\sigma^{-3}$  (solid line),  $(5 \times 10^{-5})\sigma^{-3}$  (dotted line),  $(2.5 \times 10^{-4})\sigma^{-3}$  (dash dotted line),  $(5 \times 10^{-4})\sigma^{-3}$  (dashed line), and  $(1.25 \times 10^{-3})\sigma^{-3}$  (dash dot dotted line).

$m_b^* + 5$ ). The optimal number of monomers in a bead,  $m_b^*$ , was obtained by fitting the bead distribution function around the largest peak shown in Figure 2 to the distribution function derived by Liao et al.<sup>41</sup> The growth of beads with increasing salt concentration is an indication of the ion condensation. The entropy loss due to the ion localization inside and around beads decreases with increasing salt concentration promoting ion condensation. Note that the mechanism of the bead growth with increasing salt concentration is similar to that for the bead growth with increasing polymer concentration studied by Liao et al.<sup>41</sup> To obtain the fraction of the condensed salt ions and counterions for this plot we have surrounded each monomer belonging to a bead by a sphere of radius  $r_c = 1.5\sigma$  and counted all positively charged ions with the center of mass within this cutoff distance from a monomer. The final list of the condensed ions was examined for multiple entries such that each condensed ion was counted only once. It is important to point out that for this analysis we only use the range of salt concentrations for

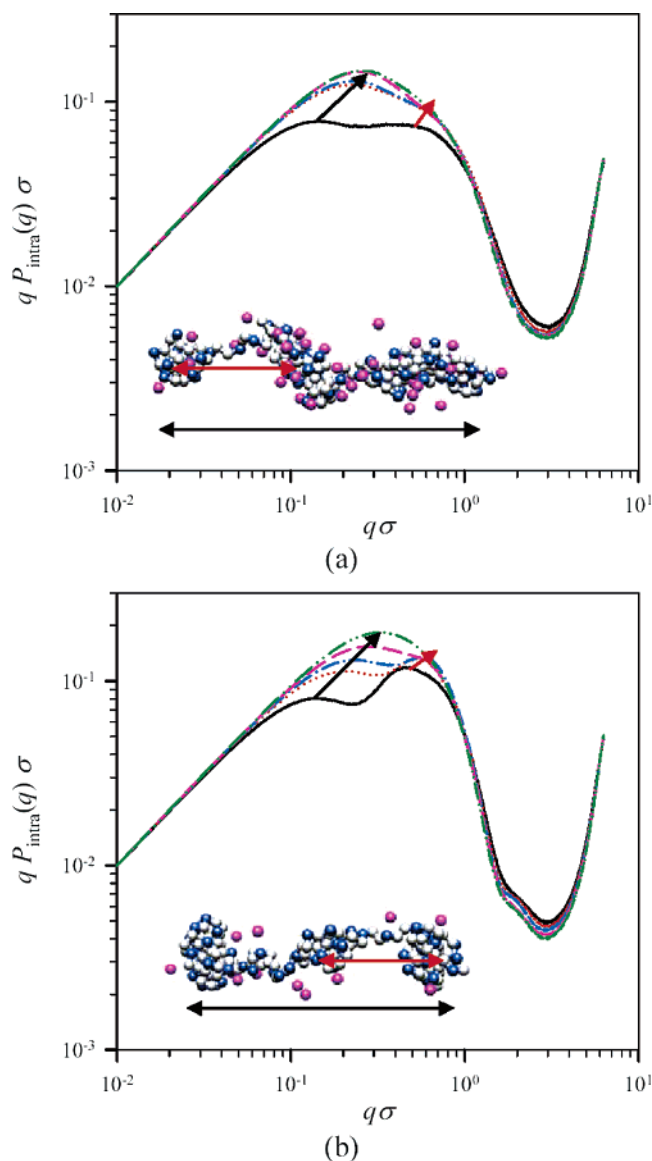


**Figure 7.** Holtzer plot of the form factor of a polyelectrolyte chain with degree of polymerization  $N_{PE} = 187$  and fraction of charged monomers  $f = 1/3$  for different values of the Bjerrum length (a)  $l_B = 3\sigma$  and (b)  $l_B = 1\sigma$  and different salt concentrations:  $c_s = 0\sigma^{-3}$  (solid line),  $(5 \times 10^{-5})\sigma^{-3}$  (dotted line),  $(2.5 \times 10^{-4})\sigma^{-3}$  (dash-dotted line),  $(5 \times 10^{-4})\sigma^{-3}$  (dashed line), and  $(1.25 \times 10^{-3})\sigma^{-3}$  (dash-dot-dotted line).

which the necklace globule is the most probable chain configuration (see Table 2).

To collapse the data for  $l_B = 1\sigma$  and  $2\sigma$  into one plot, we multiplied the optimal number of monomers  $m_b^*$  by parameter  $u = l_B/\sigma$  (see eq 7). As one can see the agreement between simulation results and eqs 7 and 8 is reasonable (see Figure 4). Two different dependences of the number of monomers in the bead on the fraction of the condensed counterions point to the possibility of the existence of two different mechanisms for the bead collapse. For the values of the Bjerrum length  $l_B = 1\sigma$  and  $2\sigma$ , the necklace formation is a result of the optimization between electrostatic repulsion between ionized groups and short-range monomer–monomer attractive interactions. However, in the case of the larger value of the Bjerrum length,  $l_B = 3\sigma$ , the necklace structure appears due to counterion condensation. In this interval of parameters there is a significant contribution of the electrostatic interactions (electrostatic repulsion and correlation-induced attraction). Note that the short-

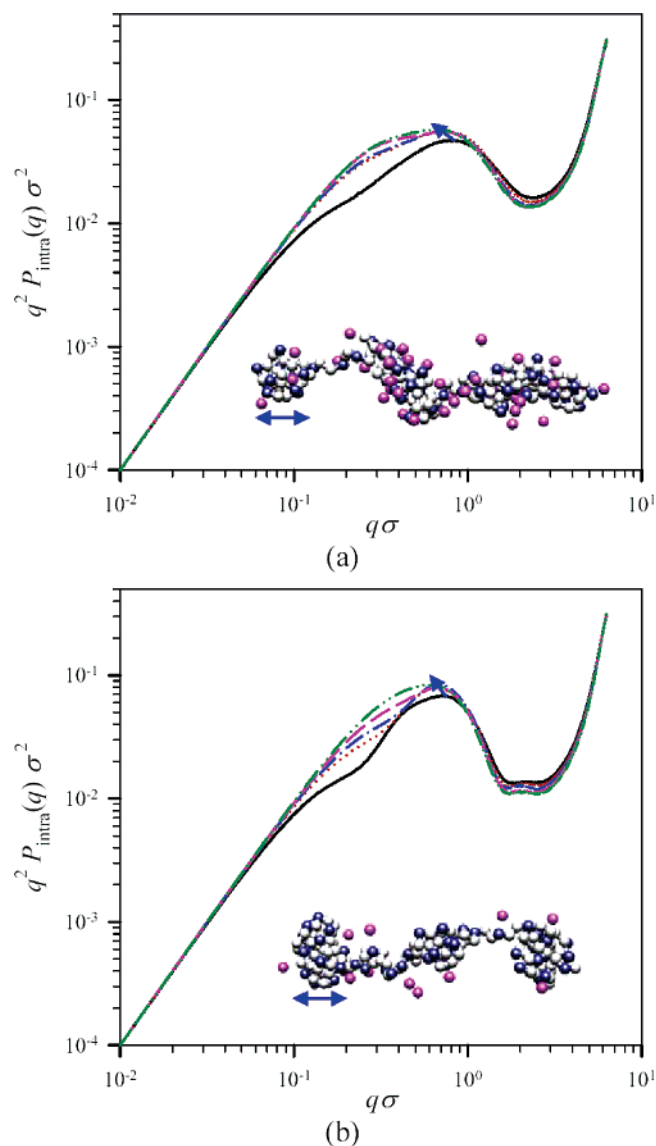


**Figure 8.** Kratky plot of the form factor of a polyelectrolyte chain with degree of polymerization  $N_{PE} = 187$  and fraction of charged monomers  $f = 1/3$  for different values of the Bjerrum length (a)  $l_B = 3\sigma$  and (b)  $l_B = 1\sigma$  and different salt concentrations:  $c_s = 0\sigma^{-3}$  (solid line),  $(5 \times 10^{-5})\sigma^{-3}$  (dotted line),  $(2.5 \times 10^{-4})\sigma^{-3}$  (dash-dotted line),  $(5 \times 10^{-4})\sigma^{-3}$  (dashed line), and  $(1.25 \times 10^{-3})\sigma^{-3}$  (dash-dot-dotted line).

range monomer–monomer attraction interactions are still important and control the crossover value of the Bjerrum length between two regimes. To further clarify this point we have performed MD simulations of a polyelectrolyte chain without added salt with the value of the monomer–monomer LJ-interaction parameter  $\epsilon_{LJ} = 0.3$  and the values of the Bjerrum length between  $1\sigma$  and  $15\sigma$ . Note that this value of the LJ-interaction parameter is close to the  $\theta$ -point condition for the polymer backbone. In these simulations a necklace structure was observed at larger values of the Bjerrum length,  $l_B \geq 10\sigma$ , which indicated that more condensed counterions were needed to force a bead formation without the help from short-range attractive interactions. The detailed study of the effect of the short-range interactions on the counterion condensation-induced bead formation will be the subject of future publications.

The simulation results for the case of the large value of the Bjerrum length,  $l_B = 3\sigma$ , are in agreement with the previous simulations by Liao et al.,<sup>41</sup> which established the correlation-induced attraction between condensed counterions and charged



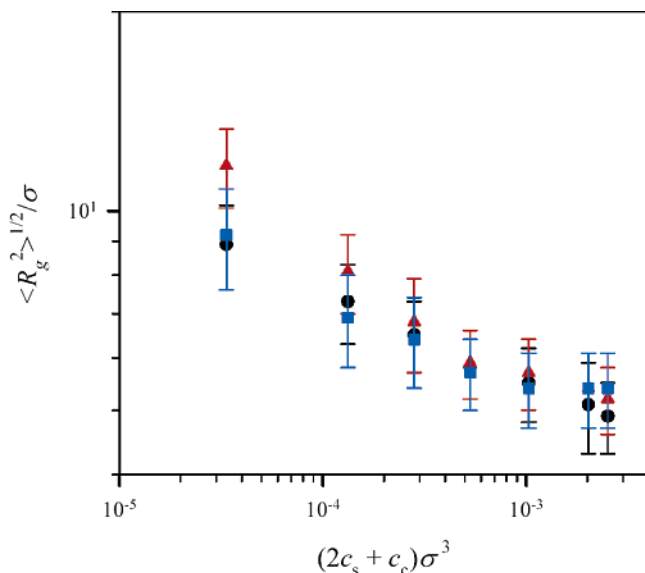


**Figure 9.** Dependence of the square-root of the mean-square average radius of gyration of a polyelectrolyte chain on salt concentration for different values of the Bjerrum length:  $l_B = 1\sigma$  (filled circles),  $2\sigma$  (filled triangles), and  $3\sigma$  (filled squares).

monomers as a driving force for the necklace formation in salt-free solutions of hydrophobic polyelectrolytes. It is important to point out that the numerical coefficients to the best fit of the simulation data to eq 8 are very close in both simulations. In our simulation this numerical coefficient is equal to 21.6 while in simulations by Liao et al.<sup>41</sup> it is 19.4. The difference between two simulations is that in Liao et al.<sup>41</sup> simulations the polymer concentration was varied while in our simulations we have changed salt concentration.

The globular beads with the number of monomers smaller than 100 have a spherical shape. For spherical beads, the bead radius of gyration  $R_g$  is proportional to  $m_b^{1/3}$ . This is in agreement with the scaling law shown in Figure 5a. However, the size  $R_g$  of the larger aggregates,  $m_b > 100$ , approaches linear dependence on the number of monomers in the aggregate. Since the sausage-like aggregates are formed by absorbing strings of monomers into beads, the typical size of the sausage can be evaluated as the size of the typical bead on the necklace  $R_g(m_b^*) \approx m_b^{*1/3}$ , times the number of beads in a sausage-like aggregate  $m_b/m_b^*$ . This leads to the size  $R_g$  of the aggregate to be proportional to  $m_b/m_b^{*2/3}$  and scaling linear with the number of monomers  $m_b$  in an aggregate. A similar trend is observed for the system with weaker electrostatic interactions,  $l_B = 1\sigma$  (see Figure 5b). However, in this case there is no well-defined interval where the aggregate size scales linearly with the number of monomers in it. This difference is due to weaker electrostatic repulsions in the system with  $l_B = 1\sigma$  in comparison with those in the system with  $l_B = 3\sigma$ . This results in smaller asymmetry of the sausage-like aggregates (see Table 2).

The evolution of the chain conformations can be monitored by analyzing the chain form factor

$$P_{\text{intra}}(q) = \frac{1}{N^2} \left\langle \sum_{ij} \exp(i\vec{q} \cdot \vec{r}_{ij}) \right\rangle = \frac{1}{N^2} \left\langle \sum_{ij} \frac{\sin(qr_{ij})}{qr_{ij}} \right\rangle \quad (9)$$

where  $\vec{q}$  is the wave vector,  $\vec{r}_{ij}$  is the vector between the  $i$ th and  $j$ th monomers on the chain, and brackets  $\langle \rangle$  denote ensemble average over all possible chain conformations. The chain form factor is shown in Figure 6. As one can see from this figure there are only weak variations in the shape of the chain form

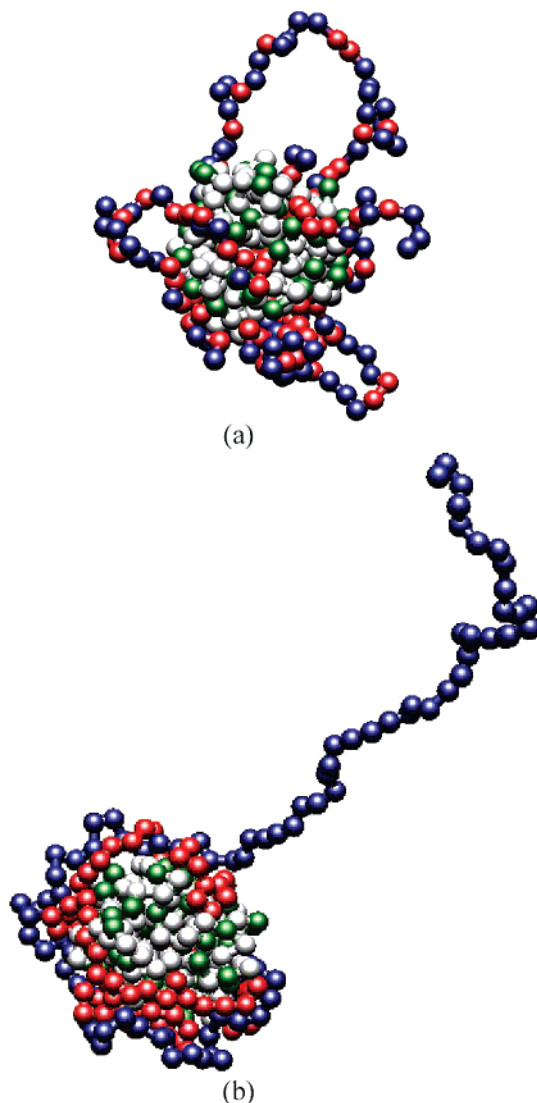


**Figure 10.** Snapshots of complex structures formed by polyelectrolyte and random polyampholyte (a) and diblock polyampholyte (b) chains. The positively charged monomers of a polyampholyte chain are shown in red and negatively charged ones are shown in blue. The negatively charged monomers of the polyelectrolyte chain are green and neutral monomers are gray.

factor in the interval of the wavenumbers  $10^{-2} < q\sigma < 1$  as salt concentration increases. The fluctuations in the necklace structures smooth out the features that one would expect to observe for the form factor of the necklace-like chains. To enhance the feature in the chain structure factor associated with beads and strings we use the Holtzer plot  $qP_{\text{intra}}(q)$  versus  $q$  (Figure 7a,b) and the Kratky plot of  $q^2P_{\text{intra}}(q)$  as function of wavenumber  $q$  (Figure 8b).

The Holtzer plot of the necklace (see Figure 7a,b) shows oscillation in the interval of the wave vectors  $0.1 < q\sigma < 1$ . These oscillations are associated with the correlations in the bead locations along the polymer backbone. The first maximum in this plot corresponds to the correlation between monomers belonging to two beads located at the chain ends. With increasing salt concentration, the magnitude of this peak increases while its position shifts toward larger  $q$  values. This shift is a result of the decrease in the number of beads per chain and shrinkage of the polyelectrolyte chain. The second maximum at the Holtzer plot is due to correlation between monomers belonging to the end beads and to the one in the middle. With increasing salt concentration, the position of the middle peak



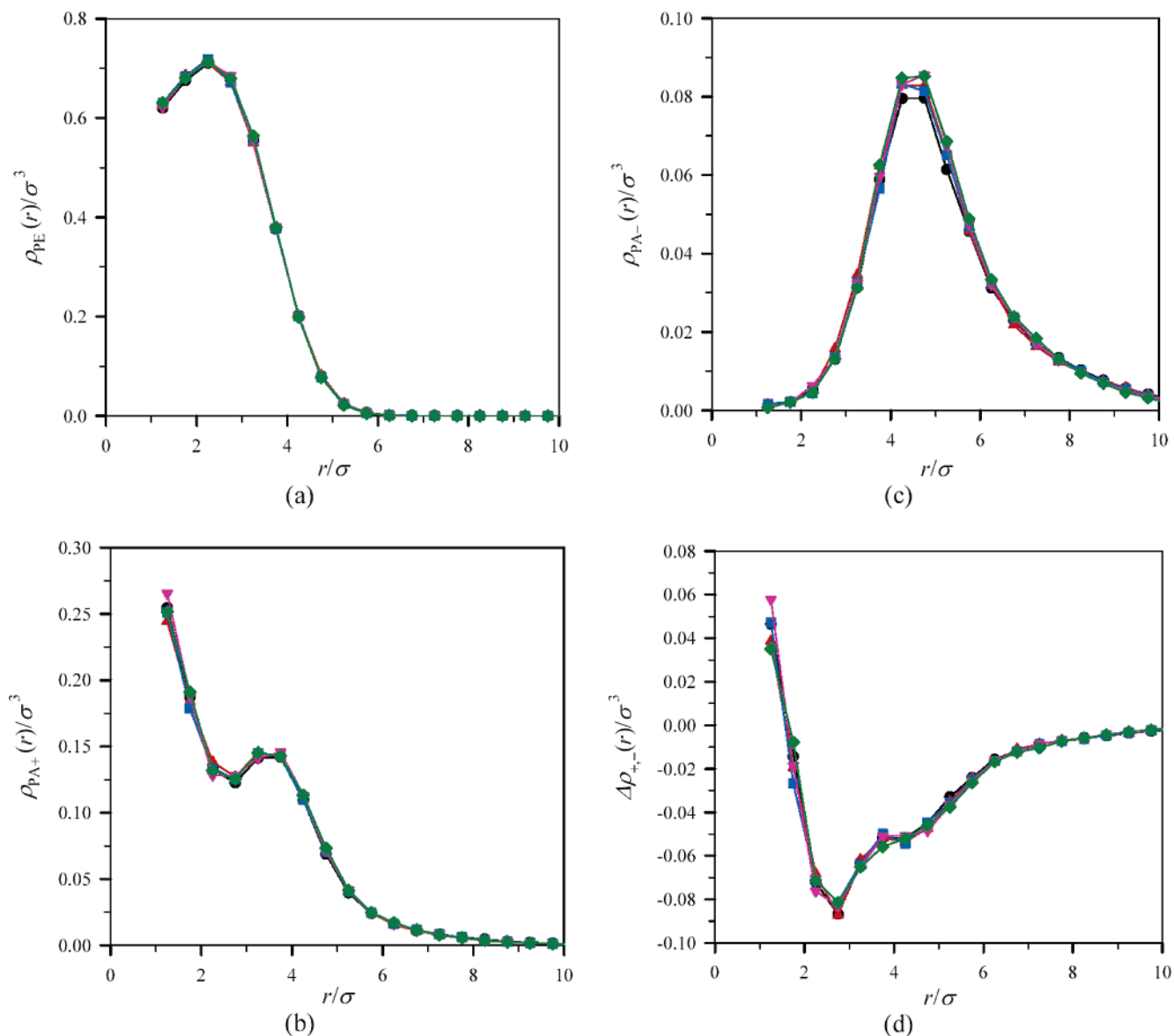


**Figure 11.** Density distribution inside complex formed by random polyampholyte and polyelectrolyte chains in the system with the value of the Bjerrum length  $l_B = 3\sigma$  at different salt concentrations:  $c_s = 0\sigma^{-3}$  (filled circles),  $(5 \times 10^{-5})\sigma^{-3}$  (filled triangles),  $(2.5 \times 10^{-4})\sigma^{-3}$  (filled squares),  $(5 \times 10^{-4})\sigma^{-3}$  (filled reverse triangles), and  $(1.25 \times 10^{-3})\sigma^{-3}$  (filled diamonds). (a) Radial density profile of monomers belonging to polyelectrolyte chain. (b) Radial density profile of positively charged monomers of a polyampholyte chain. (c) Radial density profile of negatively charged monomers of a polyampholyte chain. (d) Charge density distribution inside the core of the aggregate.

moves toward larger  $q$  values showing the decrease in the string length connecting the middle bead with the ones at chain ends. At even higher salt concentrations,  $c_s > (2.5 \times 10^{-4})\sigma^{-3}$  for  $l_B = 3\sigma$  and  $c_s > (5 \times 10^{-4})\sigma^{-3}$  for  $l_B = 1\sigma$ , this peak transforms into a shoulder. The maximum in the Kratky's plot (see Figure 8a,b) corresponds to the most probable bead size. The position of the maximum moves toward smaller  $q$  values, which is in agreement with the increase in the number of monomers in an optimal bead seen in Figure 2. Note that the peak is narrower for the system with weaker electrostatic interactions,  $l_B = 1\sigma$ . This is exactly what one would expect from the bead distribution shown in Figure 2a,b.

The size of the polyelectrolyte chain (see Figure 9) monotonically decreases with increasing salt concentration. The addition of salt ions leads to two effects: screening of the electrostatic interactions and promoting counterion condensation. With increasing salt concentration, the entropic penalty for localization of the counterions near the polymer backbone decreases making the process of counterion condensation more favorable. It is

interesting to point out that for similar salt concentrations the chain size shows nonmonotonic dependence on the value of the Bjerrum length. At low salt concentrations, an increase in the strength of the electrostatic interactions (the value of the Bjerrum length) first leads to an increase in the chain size (see points for  $l_B = 2\sigma$ ). This is due to stronger electrostatic repulsion between ionized groups on the polymer backbone. However, as the strength of the electrostatic interactions increases further, the counterion condensation reduces the effective charge on the polyelectrolyte chain forcing it to shrink. More counterions are localized near polymer backbone in the systems with stronger electrostatic interactions leading to an additional attraction (correlation-induced attraction) between charged monomers. This additional attraction causes chain collapse. However, this nonmonotonic dependence of the chain size disappears at high salt concentration where the polyelectrolyte chain adopts a globule-like conformation. At this range of salt concentrations the short-range monomer–monomer interactions control chain conformations.

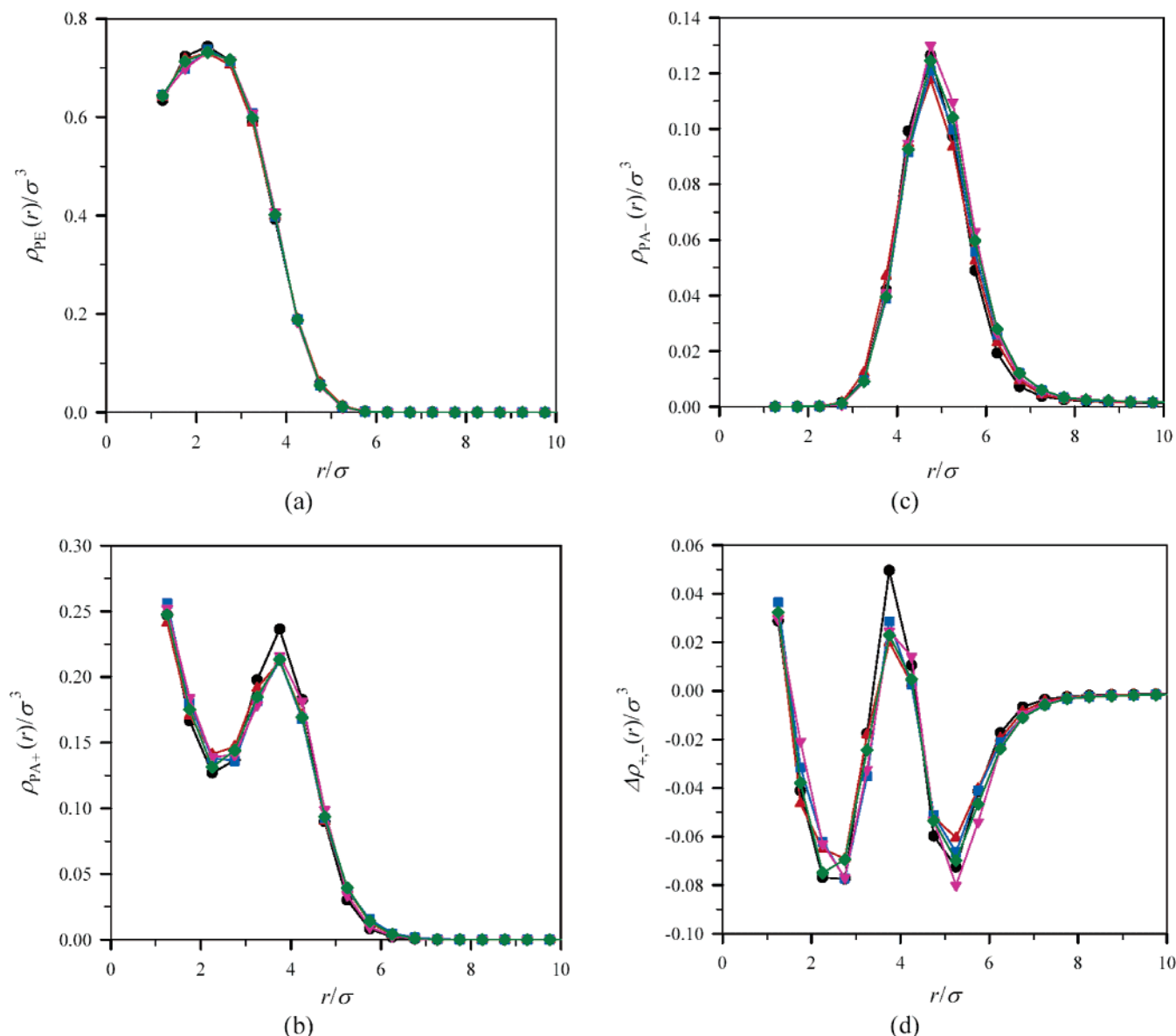


**Figure 12.** Density distribution inside complex formed by diblock polyampholyte and polyelectrolyte chains in the system with the value of the Bjerrum length  $l_B = 3\sigma$  at different salt concentrations:  $c_s = 0\sigma^{-3}$  (filled circles),  $(5 \times 10^{-5})\sigma^{-3}$  (filled triangles),  $(2.5 \times 10^{-4})\sigma^{-3}$  (filled squares),  $(5 \times 10^{-4})\sigma^{-3}$  (filled reverse triangles), and  $(1.25 \times 10^{-3})\sigma^{-3}$  (filled diamonds). (a) Radial density profile of monomers belonging to polyelectrolyte chain. (b) Radial density profile of positively charged monomers of a polyampholyte chain. (c) Radial density profile of negatively charged monomers of a polyampholyte chain. (d) Charge density distribution inside the core of the aggregate.

#### 4. Complex Formation between Polyelectrolyte and Polyampholyte Chains

Upon forming a complex with both random (Figure 10 a) and diblock (Figure 10 b) polyampholytes a polyelectrolyte chain changes its necklace conformation by forming one huge bead. The collapse of the polyelectrolyte chain occurs due to neutralization of the polyelectrolyte charge by polyampholytes. In the case of the random polyampholyte, the more positively charged sections of the chain form the core of the globular bead while more negatively charged chain sections form loops surrounding the collapsed core of the aggregate. In the case of diblock polyampholyte, the positively charged block is absorbed into the core of the aggregate, a part of the negatively charged block wraps around the core with a substantial section of the negatively charged block sticking out from the collapsed center of the aggregate. These structures appear as a result of optimization of the net electrostatic energy of the complex and short-range attractive interactions between monomers of the

polyelectrolyte chain. The additional adsorption of the negatively charged monomers of the diblock polyampholyte chain on the core of the aggregate is due to the charge mismatch between positively charged monomers on a polyampholyte and negatively charged monomers on a polyelectrolyte. There are 63 negatively charged monomers on the polyelectrolyte chain and 93 oppositely charged monomers on the diblock polyampholyte, which leaves an extra 30 positively charged monomers that should be compensated by the negatively charged monomers of the diblock polyampholyte chain to minimize the net core charge. Below we will present the detailed analysis of the effect of the salt concentration on the complex structure formed by random and diblock polyampholytes with a polyelectrolyte chain in the system with the Bjerrum length  $l_B = 3\sigma$ . The complex structures formed by these polymers in the system with weaker electrostatic interactions,  $l_B = 2\sigma$  and  $1\sigma$ , show qualitatively similar salt concentration dependencies as one described below and will not be discussed here.

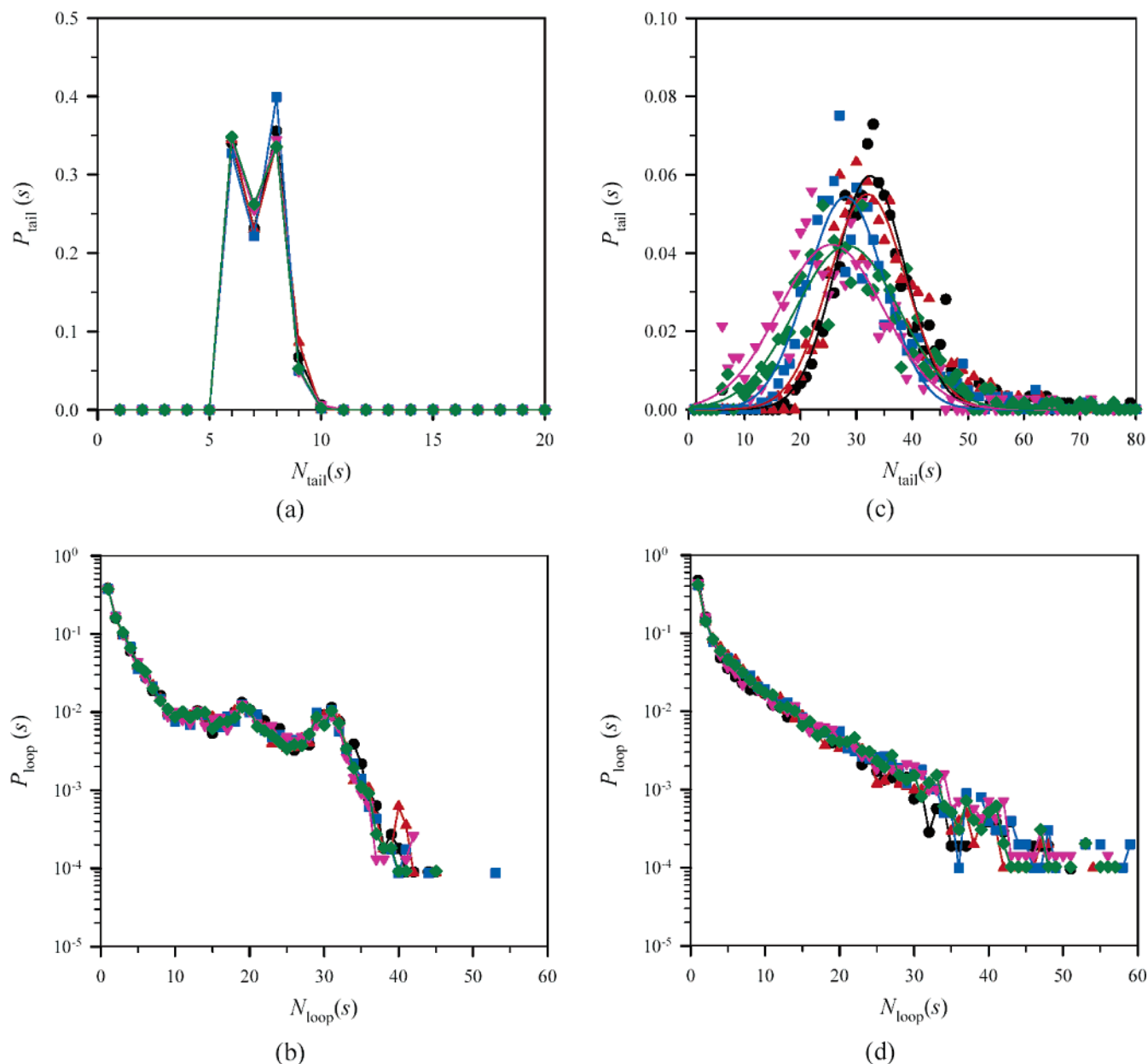


**Figure 13.** Tail and loop distribution functions in the system with the value of the Bjerrum length  $l_B = 3\sigma$  at different salt concentrations:  $c_s = 0\sigma^{-3}$  (filled circles),  $(5 \times 10^{-5})\sigma^{-3}$  (filled triangles),  $(2.5 \times 10^{-4})\sigma^{-3}$  (filled squares),  $(5 \times 10^{-4})\sigma^{-3}$  (filled reverse triangles), and  $(1.25 \times 10^{-3})\sigma^{-3}$  (filled diamonds). (a) Tail and (b) loop distribution function for random polyampholyte–polyelectrolyte complexes and (c) tail and (d) loop distribution function for diblock polyampholyte–polyelectrolyte complexes.

The dense core of the aggregate is comprised from monomers belonging to both polyelectrolyte and polyampholyte chains (see Figures 11 and 12). The origin of the coordinate system for the density distribution functions shown in Figures 11 and 12 is located at the center of mass of the polyelectrolyte chain. The center of the core of the aggregates has an excess of the positively charged monomers belonging to the polyampholyte chain (see Figures 11a,b and 12a,b). The concentration of the positively charged monomers oscillates throughout the core (see Figures 11b and 12b). It has a maximum at the center of the core then it decreases reaching the first minimum at  $r \approx 2\sigma$ . The decrease in the concentration of positively charged monomers is offset by the increase in polyelectrolyte concentration, which reaches a maximum at about the same distance from the core center. The second maximum in concentration of the positively charged monomers is located at  $r \approx 3.5\sigma$ . It is worth pointing out that the oscillations in concentration of the positively charged monomers belonging to a polyampholyte

chain are more pronounced in the case of the diblock polyampholyte. The negatively charged monomers of a polyampholyte chain are located at the outer boundary of the core (see Figures 11c and 12c). These distributions of the monomer densities throughout the core result in the charge density oscillations seen in Figures 11d and 12d. Thus, the core of the complex formed by polyampholyte and polyelectrolyte chains has a layered structure. In the case of diblock polyampholytes, there are four layers inside the core while the system with random polyampholytes shows only two layers.

Additional information about complex structure can be obtained by analyzing tail and loop distribution functions. A tail is defined as a sequence of bonds beginning from the chain end to the first bead in contact with a polyelectrolyte. Below we will assume that the two beads are in contact with each other if the distance between them is smaller than  $1.1\sigma$ . A loop is defined as a sequence of bonds between two nearest along the polymer backbone beads that are in contact with a polyelec-

trolyte. The minimum length of the loop is equal to 1 and the longest loop can have  $N_{\text{PA}} - 1$  bonds in it. The probability distribution functions of tail  $P_{\text{tail}}(s)$  and loop  $P_{\text{loop}}(s)$  with  $s$  bonds are defined as follows

$$P_{\text{tail}}(s) = \frac{N_{\text{tail}}(s)}{\sum_i N_{\text{tail}}(i)} \quad (10)$$

and

$$P_{\text{loop}}(s) = \frac{N_{\text{loop}}(s)}{\sum_i N_{\text{loop}}(i)} \quad (11)$$

where  $N_{\text{tail}}(i)$  and  $N_{\text{loop}}(i)$  are the total numbers of tails and loops with  $i$  bonds observed during the simulation runs. Panels a–d of Figure 13 show the dependence of the tail  $P_{\text{tail}}(s)$  and loop  $P_{\text{loop}}(s)$  probability distribution functions on salt concentration for random and diblock polyampholyte chains. For random polyampholytes the tail distribution function has two peaks located at  $s = 6$  and 8 (see Figure 13a). These two peaks correspond to two tails formed by the two ends of a randomly charged polyampholyte chains. The position of these peaks is independent of the salt concentration. However, their magnitudes slowly decrease indicating screening of the electrostatic repulsion between charged monomers forming tails and ones forming a core of an aggregate. There is only one peak in the tail distribution function for a complex formed by diblock polyampholyte (see Figure 13c). This is in agreement with the complex structure seen in Figure 10b showing the large section of the negatively charged block being expelled from the core of the complex forming a long tail. With increasing salt concentration, the number of monomers in a tail decreases as a result of the screening of the electrostatic repulsion between polyelectrolytes forming a core of the complex and similarly charged monomers in the tail.

The loop distribution functions for random polyampholyte first decrease with increasing the number of bonds in a loop then show oscillations at the interval of the number of bonds per loop between 10 and 40 bonds. This loop distribution function reveals that the majority of contacts in a complex are formed by consecutive monomers along the polymer backbone. The oscillations in the loop distribution function indicate that there are also large loops that accumulate negatively charged monomers. This loop distribution function is in agreement with the flowerlike complex structure seen in Figure 10a. For diblock polyampholyte the probability of finding a large loop monotonically decreases. This confirms our observation that the oppositely charged block of a polyampholyte chain is in contact (wraps around) with the oppositely charged collapsed polyelectrolyte (see Figure 10b).

The wrapping of the polyampholyte chain around a core of the complex formed by a diblock polyampholyte and a polyelectrolyte can be followed by considering the variations of the cosine of an angle  $\theta$  between the radius vector pointing from the center of a core to the first monomer forming a tail and the radius vector pointing toward the  $m$ th monomer from it (see inset in Figure 14). The value of the cosine first decreases with increasing the number of monomers from the tail contact point. It reaches the minimum value  $-0.5$ , which corresponds to a turn by  $120^\circ$  at  $m = 30$ . Then it starts to increase again. The

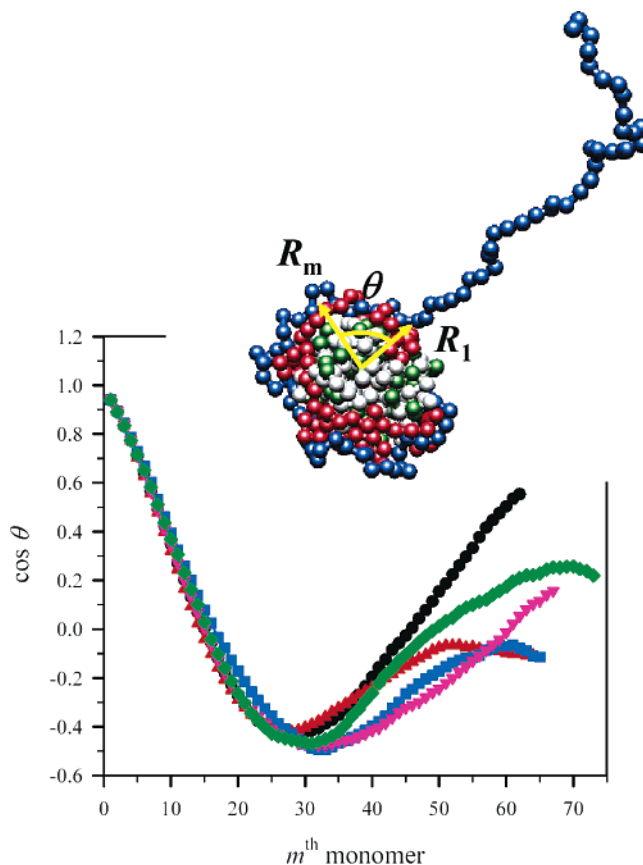


**Figure 14.** Dependence of the cosine of the angle between the first monomer forming tail and the  $m$ th monomer from it on salt concentration for diblock polyampholytes with  $l_B = 3\sigma$  at different salt concentrations:  $c_s = 0\sigma^{-3}$  (filled circles),  $(5 \times 10^{-5})\sigma^{-3}$  (filled triangles),  $(2.5 \times 10^{-4})\sigma^{-3}$  (filled squares),  $(5 \times 10^{-4})\sigma^{-3}$  (filled reverse triangles), and  $(1.25 \times 10^{-3})\sigma^{-3}$  (filled diamonds). The inset shows the definition of an angle  $\theta$ .

increase in the value of the cosine is the indication of the beginning of the turn around. Note that the wrapping section of the diblock polyampholyte does not make a large circle around the core. This follows from the fact that the minimum value of the cosine is equal to  $-0.5$ . The overall shape of the wrapped section of the diblock polyampholyte is similar to a baseball thread. This arrangement of the negatively charged block on the complex surfaces minimizes the intrablock electrostatic repulsion. The salt concentration does not have a dramatic effect on the wrapping of a diblock polyampholyte chain around the core of the complex (see Figure 14). It mostly influences the values of the cosine function for large  $m$ -values that correspond to the monomers located in space close to the initial tail contact point.

As we have shown in the previous section the Holtzer plot of the necklace (see Figure 7a,b) is very sensitive to the conformational changes. There are oscillations in the magnitude of the function  $qP_{\text{intra}}(q)$  that correspond to correlations in the bead distribution along the polymer backbone. Thus, it should be possible to use the Holtzer plot of a polyelectrolyte chain for monitoring conformational changes as a polyelectrolyte chain forms a complex with a polyampholyte. Indeed panels a and b of Figures 15 show the disappearance of the oscillations in the function  $qP_{\text{intra}}(q)$  at the intermediate wave vectors range associated with the correlations between monomers belonging to beads (see Figure 7a,b) confirming formation of one huge bead.



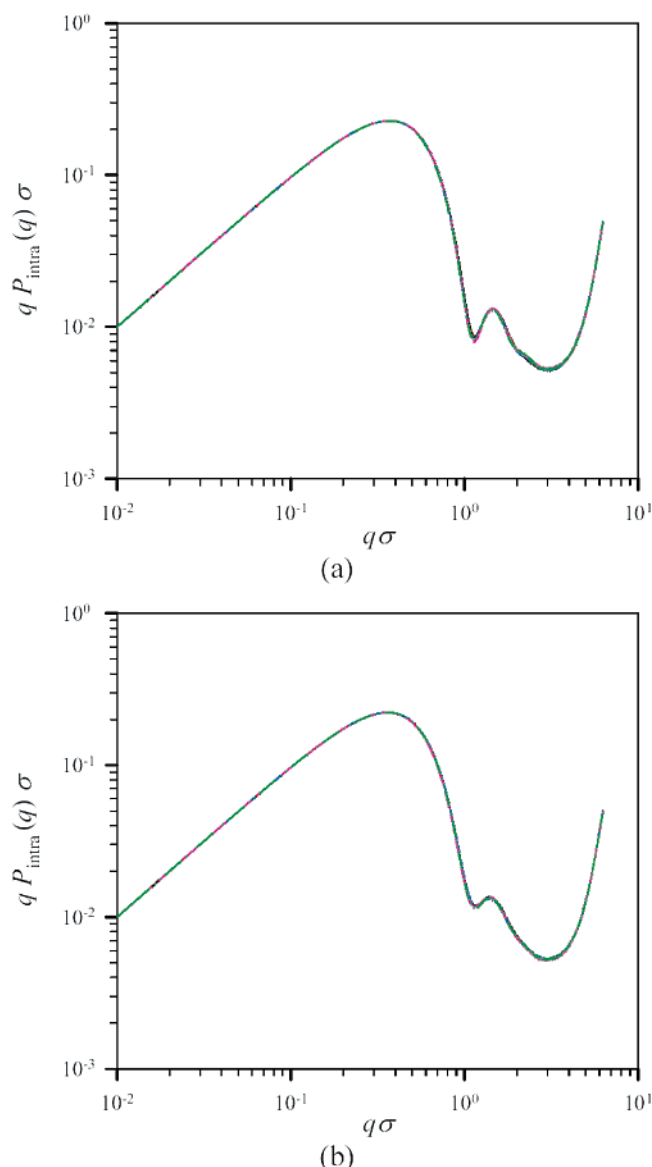


**Figure 15.** Holtzer plot of the form factor of a polyelectrolyte chain with degree of polymerization  $N_{PE} = 187$ , fraction of charged monomers  $f = 1/3$ , and the value of the Bjerrum length  $l_B = 3\sigma$  in a complex with random (a) and diblock (b) polyampholytes at different salt concentrations:  $c_s = 0\sigma^{-3}$  (solid line),  $(5 \times 10^{-5})\sigma^{-3}$  (dotted line),  $(2.5 \times 10^{-4})\sigma^{-3}$  (dash dotted line),  $(5 \times 10^{-4})\sigma^{-3}$  (dashed line), and  $(1.25 \times 10^{-3})\sigma^{-3}$  (dash dot dotted line).

## 5. Conclusions

We have studied how the salt concentration, strength of the electrostatic interactions, and association with polyampholyte chains with different sequences of the charged monomers along the polymer backbone can change conformations of hydrophobic (solvophobic) polyelectrolytes. The results of the molecular dynamics simulations can be understood by assuming the existence of two different mechanisms that could lead to formation of the necklace structure in a polyelectrolyte chain. For the values of the Bjerrum length  $l_B = 1\sigma$  and  $2\sigma$  the necklace structure appears as a result of competition between short-range monomer–monomer attractive interactions and electrostatic repulsion between uncompensated charges. However, for the value of the Bjerrum length  $l_B = 3\sigma$  the necklace structure appears due to counterion condensation and is due to the optimization of the correlation-induced attraction between charged monomers and condensed counterions, and electrostatic

repulsion between uncompensated charges on the polymer backbone. Note that the short-range monomer–monomer attractions still play an important role in determining the crossover value of the Bjerrum length between two regimes. The results for the second regime are in agreement with the results of the molecular dynamics simulations by Liao et al.<sup>41</sup> of the salt-free polyelectrolyte solutions. The fitting parameters to eq 8 relating the number of monomers in the optimal bead  $m_b^*$  with the fraction of the condensed counterions  $x$  are very close in both simulations. This should not be surprising since the fraction of the condensed counterions depends on the counterion configurational entropy, which can be changed either by varying the polymer concentration or by adding salt.

Complexation between a polyampholyte and a polyelectrolyte chain proceeds through the release of counterions condensed on the polyelectrolyte backbone. These counterions are substituted by the positively charged monomers of a polyampholyte chain. The complex structure shows strong correlation with the charge sequence along the polymer backbone. In the case of a random polyampholyte the complex has a flowerlike structure of the dense core surrounded by loops. The core of the aggregate contains more positively charged polyampholyte chain sections and a whole polyelectrolyte chain. The more negatively charge section of the polyampholyte form loops surrounding the core of the aggregate. The diblock polyampholyte has a tadpole-like structure with the tail of the tadpole containing part of the negatively charged block. The remaining part of the negatively charged block is wrapped around the head of the tadpole. In both systems there are charged density oscillations inside the core. In the case of random polyampholytes the center of the core has an excess of positively charged monomers, which is surrounded by the layer of negatively charged ones. The core of the complex formed by the diblock polyampholyte has four charge alternating layers with an excess of the positively charged monomers in the core center. These complex structures persisted throughout the entire studied salt concentration range and show no qualitative changes with varying the strength of the electrostatic interactions (the value of the Bjerrum length).

**Acknowledgment.** This work was supported by the National Science Foundation under Grant DMR-0305203.

## References and Notes

- (1) Dobrynin, A. V.; Rubinstein, M. *Prog. Polym. Sci.* **2005**, *30*, 1049–1118.
- (2) Grosberg, A. Y.; Nguyen, T. T.; Shklovskii, B. I. *Rev. Mod. Phys.* **2002**, *74*, 329–345.
- (3) Cooper, C. L.; Dubin, P. L.; Kayitmazer, A. B.; Turksen, S. *Curr. Opin. Colloid Interface Sci.* **2005**, *10*, 52–78.
- (4) Dubin, P. L.; Farinato, R. S. *Colloid-Polymer Interactions: From Fundamentals to Practice*; Wiley-Interscience: New York, 1999.
- (5) *Multilayer Thin Films*; Wiley-VCH: New York, 2003.
- (6) Mathews, C. K.; Van Holde, K. E.; Ahern, K. G. *Biochemistry*; Benjamin/Cummings: San Francisco, CA, 2000.
- (7) Bloomfield, V. A. *Biopolymers* **1997**, *44*, 269–282.
- (8) Dubin, P.; Bock, J.; Davis, R.; Schluz, D. N.; Thies, C. *Macromolecular Complexes in Chemistry and Biology*; Springer-Verlag: Dusseldorf, Germany, 1994.
- (9) Raspud, E.; Olvera de la Cruz, M.; Sikorav, J.-L.; Livolant, F. *Biophys. J.* **1998**, *74*, 381–393.
- (10) Butler, J. C.; Angelini, T.; Tang, J. X.; Wong, G. C. L. *Phys. Rev. Lett.* **2003**, *91*, 028301–1–4.
- (11) Burak, Y.; Ariel, G.; Andelman, D. *Biophys. J.* **2003**, *85*, 2100–2110.
- (12) Needleman, D. J.; Ojeda-Lopez, M. A.; Raviv, U.; Miller, H. P.; Willson, L.; Safinya, C. R. *PNAS* **2004**, *101*, 16099–16103.
- (13) Borukhov, L.; Bruinsma, R. F.; Gelbart, W. M.; Liu, A. J. *Proc. Natl. Acad. Sci. U.S.A.* **2005**, *102*, 3673–3678.
- (14) de Vries, R. *Biophys. J.* **2001**, *80*, 1186–1194.

- (15) Iwataki, T.; Kidoaki, S.; Sakaue, T.; Yoshikawa, K.; Abramchuk, S. S. *J. Chem. Phys.* **2004**, *120*, 4004–4011.
- (16) Kwon, H. J.; Kakugo, A.; Shikinaka, K.; Osada, Y.; Gong, J. P. *Biomacromolecules* **2005**, *6*, 3005–3009.
- (17) McLoughlin, D.; Delsanti, M.; Tribet, C.; Langevin, D. *Europhys. Lett.* **2005**, *69*, 461–467.
- (18) Stevens, M. J. *Biophys. J.* **2001**, *80*, 485A.
- (19) Tang, J. X.; Kas, J. A.; Shah, J. V.; Janmey, P. A. *Eur. Biophys. J. Biophys. Lett.* **2001**, *30*, 477–484.
- (20) Zilman, A. G.; Safran, S. A. *Europhys. Lett.* **2003**, *63*, 139–145.
- (21) Zribi, O. V.; Kyung, H.; Golestanian, R.; Liverpool, T. B.; Wong, G. C. L. *Europhys. Lett.* **2005**, *70*, 541–547.
- (22) Decher, G. Polyelectrolyte Multilayers, an Overview. In *Multilayer Thin Films*; Decher, G., Schlenoff, J. B., Eds.; Wiley-VCH: New York, 2003; pp 1–46.
- (23) Caruso, F. *Adv. Mater.* **2001**, *13*, 11–22.
- (24) Dubin, P. L.; Gao, J.; Mattison, K. *Sep. Purif. Methods* **1994**, *23*, 1–16.
- (25) Dobrynin, A. V.; Colby, R.; Rubinstein, M. *J. Polym. Sci., Part B: Polym. Phys.* **2004**, *42*, 3513–3538.
- (26) Carlsson, F.; Linse, P.; Malmsten, M. *J. Phys. Chem. B* **2001**, *105*, 9040–9049.
- (27) Carlsson, F.; Malmsten, M.; Linse, P. *J. Am. Chem. Soc.* **2003**, *125*, 3140–3149.
- (28) Cheatham, T. E. I.; Young, M. A. *Biopolymers (Nucleic Acid Sci.)* **2001**, *56*, 232–256.
- (29) Giudice, E.; Lavery, R. *Acc. Chem. Res.* **2002**, *35*, 350–357.
- (30) Jeon, J.; Dobrynin, A. V. *Macromolecules* **2005**, *38*, 5300–5312.
- (31) Jeon, J.; Dobrynin, A. V. *Phys. Rev. E* **2003**, *67*, 061803-1-15.
- (32) Dobrynin, A. V.; Rubinstein, M.; Obukhov, S. P. *Macromolecules* **1996**, *29*, 2974–2979.
- (33) Dobrynin, A. V.; Rubinstein, M. *Macromolecules* **1999**, *32*, 915–922.
- (34) Solis, F. J.; de la Cruz, M. O. *Macromolecules* **1998**, *31*, 5502–5506.
- (35) Micka, U.; Kremer, K. *Europhys. Lett.* **2000**, *49*, 189–195.
- (36) Micka, U.; Holm, C.; Kremer, K. *Langmuir* **1999**, *15*, 4033–4044.
- (37) Lyulin, A. V.; Dunweg, B.; Borisov, O. V.; Darinskii, A. A. *Macromolecules* **1999**, *32*, 3264–3278.
- (38) Limbach, H. J.; Holm, C. *Comput. Phys. Commun.* **2002**, *147*, 321–324.
- (39) Limbach, H. J.; Holm, C. *J. Phys. Chem. B* **2003**, *107*, 8041–8055.
- (40) Limbach, H. J.; Holm, C.; Kremer, K. *Macromol. Symp.* **2004**, *211*, 43–53.
- (41) Liao, Q.; Dobrynin, A. V.; Rubinstein, M. *Macromolecules* **2006**, *39*, 1920.
- (42) Frenkel, D.; Smit, B. *Understanding Molecular Simulations*; Academic Press: San Diego, CA, 2001.
- (43) Pollock, E. L.; Glosli, J. *Comput. Phys. Commun.* **1996**, *95*, 93–110.
- (44) Dobrynin, A. V. Molecular simulations of charged polymers. In *Simulation methods for polymers*; Kotelyanskii, M., Theodorou, D. N., Eds.; Marcel Dekker: New York, 2004; pp 259–312.
- (45) Plimpton, S. *LAMMPS User's Manual*; Sandia National Lab, 2005.